JAMES | Journal of Advances in Modeling Earth Systems®

RCEMIP-ACI: Aerosol-Cloud Interactions in a Multimodel Ensemble of Radiative-Convective Equilibrium Simulations

Guy Dagan[1] , **Susan C. van den Heever[2]** , **Philip Stier[3]** , **Tristan H. Abbott[4]** , **Christian Barthlott[5]** , **Jean-Pierre Chaboureau[6]** , **Jiwen Fan[7]** , **Stephan de Roode[8]** , **Blaž Gasparini[9]** , **Corinna Hoose[5]** , **Fredrik Jansson[8]** , **Gayatri Kulkarni[10]** , **Gabrielle R. Leung[2]** , **Suf Lorian[1]** , **Thara Prabhakaran[10]** , **David M. Romps[11]** , **Denis Shum[1]** , **Mirjam Tijhuis[12]** , **Chiel C. van Heerwaarden[12]** , **Allison A. Wing[13]** , and **Yunpeng Shan[7]**

[1]Fredy and Nadine Herrmann Institute of Earth Sciences, Hebrew University, Jerusalem, Israel, [2]Department of Atmospheric Science, Colorado State University, Fort Collins, CO, USA, [3]Atmospheric, Oceanic and Planetary Physics, Department of Physics, University of Oxford, Oxford, UK, [4]Program in Atmospheric and Oceanic Sciences, Princeton University, Princeton, NJ, USA, [5]Institute of Meteorology and Climate Research Troposphere Research (IMKTRO), Karlsruhe Institute of Technology, Karlsruhe, Germany, [6]LAERO, Université de Toulouse, CNRS, IRD, Toulouse, France, [7]Environmental Science Division, Argonne National Laboratory, Lemont, IL, USA, [8]Department of Geoscience and Remote Sensing, Delft University of Technology, Delft, The Netherlands, [9]Department of Meteorology and Geophysics, Faculty of Earth Sciences, Geography and Astronomy, University of Vienna, Vienna, Austria, [10]Indian Institute of Tropical Meteorology, Pune, India, [11]Department of Earth and Planetary Science, University of California, Berkeley, CA, USA, [12]Meteorology and Air Quality Group, Wageningen University & Research, Wageningen, The Netherlands, [13]Department of Earth, Ocean and Atmospheric Science, Florida State University, Tallahassee, FL, USA

Abstract Aerosol-cloud interactions are a persistent source of uncertainty in climate research. This study presents findings from a model intercomparison project examining the impact of aerosols on clouds and climate in convection-permitting radiative-convective equilibrium (RCE) simulations. Specifically, 11 different modeling teams conducted RCE simulations under varying aerosol concentrations, domain configurations, and sea surface temperatures (SSTs). We analyze the response of domain-mean cloud and radiative properties to imposed aerosol concentrations across different SSTs. Additionally, we explore the potential impact of aerosols on convective aggregation and large-scale circulation in large-domain simulations. The results reveal that the cloud and radiative responses to aerosols vary substantially across models. However, a common trend across models, SSTs, and domain configurations is that increased aerosol loading tends to suppress warm rain formation, enhance cloud water content in the mid-troposphere, and consequently increase mid-tropospheric humidity and upper-tropospheric temperature, thereby impacting static stability. The warming of the upper troposphere can be attributed to reduced lateral entrainment effects due to the higher environmental humidity in the mid-troposphere. However, models do not agree on aerosol impacts on convective updraft velocity based on the preliminary examination of high-percentiles of vertical velocity at a single mid-tropospheric layer (500 hPa). In large-domain simulations, where convection tends to self-organize, aerosol loading does not consistently influence self-organization but tends to reduce the intensity of large-scale circulation forming between convective clusters and dry regions. This reduction in circulation intensity can be explained by the increase in static stability due to the upper tropospheric warming.

Plain Language Summary Aerosols, small particles suspended in the atmosphere, influence cloud properties by acting as nuclei for cloud droplet formation. These aerosol-cloud interactions (ACI) introduce uncertainties in climate research, making it essential to improve our understanding of them. This paper presents findings from a model intercomparison project that examines the impact of aerosols on clouds and climate in simulations that directly represent cloud processes under idealized equilibrium climate conditions. We show that cloud responses to aerosols vary substantially across models, though certain consistent responses emerge. Specifically, increased aerosol loading generally suppresses initial rain formation, which in turn alters the thermodynamic conditions of the atmosphere. We also discuss how these thermodynamic changes influence the large-scale atmospheric circulation.

Visualization: Guy Dagan
Writing – original draft: Guy Dagan
Writing – review & editing: Guy Dagan, Susan C. van den Heever, Philip Stier, Christian Barthlott, Jean-Pierre Chaboureau, Jiwen Fan, Stephan de Roode, Blaž Gasparini, Fredrik Jansson, Suf Lorian, Denis Shum, Chiel C. van Heerwaarden, Allison A. Wing

1. Introduction

Human activities release aerosols and precursor gases into the atmosphere, many of which act as cloud condensation nuclei (CCN), affecting cloud droplet formation. Consequently, cloud droplet number concentrations (CDNC) generally increase with rising aerosol levels (Squires, 1958), affecting cloud radiative (Twomey, 1974) and macro-physical (Albrecht, 1989; Wall et al., 2022) properties, thereby influencing climate via radiative effects (Bellouin et al., 2020) and the hydrological cycle (Stier et al., 2024). These aerosol-cloud interactions (ACI) introduce substantial uncertainties in climate projections (Bellouin et al., 2020; Forster et al., 2024), underscoring the importance of improving our understanding of them.

An increase in CDNC due to elevated CCN levels reduces mean droplet size and raises cloud albedo for a given liquid water path, as described by the Twomey effect (Twomey, 1974). Smaller droplets, with a more narrow size distribution, can delay rain formation, potentially increasing cloud coverage and water content (Albrecht, 1989; Bellouin et al., 2020; Wall et al., 2022). However, uncertainties surrounding these effects remain substantial (Stevens & Feingold, 2009). For instance, higher CDNC may also reduce cloudiness due to a faster droplet evaporation at cloud edges, and more efficient mixing with the surrounding environment (Dagan et al., 2017; Glassmeier et al., 2021). Thus, the overall net impact of aerosols on clouds remains an open question.

While these mechanisms primarily pertain to shallow clouds, aerosols can also influence deep convective clouds. Delays in warm rain formation, which lead to larger amounts of liquid water being transported above the freezing level, can enhance latent heat release through freezing, thereby strengthening updrafts and potentially invigorating convective cloud development (Rosenfeld et al., 2008; Williams et al., 2002). However, this "cold-phase invigoration" mechanism is substantial only if the added water loading's negative impact on buoyancy does not offset the positive latent heating effect (Igel & van den Heever, 2021; A. C. Varble et al., 2023).

Moreover, under equilibrium conditions, as simulated in this work, the tropical atmospheric temperature profile is governed by convection (Sobel et al., 2001). As a result, buoyancy and vertical velocities in clouds are unlikely to be influenced by the amount of latent heating at the upper levels (Seeley & Romps, 2016). In the warm, liquid-dominated regions of deep convective clouds, increased droplet concentrations may improve condensation efficiency, further invigorating clouds ("warm-phase invigoration" or better "condensational invigoration"; (Fan et al., 2018; Igel & van den Heever, 2021; Koren et al., 2014; Lebo, 2018; Sheffield et al., 2015)). However, these mechanisms remain a topic of debate, and their overall importance is still unclear (Romps et al., 2023; Stier et al., 2024; A. Varble, 2018; A. C. Varble et al., 2023).

In addition to the impact of aerosols on cloud-scale dynamics, further research emphasizes the role of aerosol-induced large-scale environmental changes (Abbott & Cronin, 2021; Dagan et al., 2023). Specifically, the suppression of warm rain formation by aerosols leads to more liquid water remaining within clouds and more water vapor persisting in the surrounding environment, resulting in a net humidification of the lower to mid-troposphere (Abbott & Cronin, 2021). This enhanced environmental humidity reduces the efficiency of entrainment-driven evaporative cooling, allowing rising cloud parcels to remain warmer. Due to the weak temperature gradient approximation in the tropics, this warming of convective parcels also translates into warming of the upper free troposphere (Abbott & Cronin, 2021). These changes in the vertical temperature structure modify the atmospheric static stability and can, in turn, influence large-scale circulation patterns (Dagan et al., 2023).

In addition, this tropospheric warming and enhanced static stability affect anvil cloud cover in ways similar to the iris-stability mechanism associated with sea surface temperature changes (Bony et al., 2016; Lorian & Dagan, 2024). In addition, given the strong coupling between clouds and large-scale atmospheric circulation (Bony et al., 2015), aerosol-driven modifications in cloud properties can influence large-scale circulation and cloud regimes' development (Christensen et al., 2020; Dagan et al., 2023; Goren et al., 2019). For example, delays in warm rain formation can prolong cloud regime transitions in the tropics (Christensen et al., 2020; Goren et al., 2019). This delay is expected to increase water vapor transport to other regions, potentially impacting circulation patterns on a large scale (Abbott & Cronin, 2021; Dagan et al., 2023). In addition to the large scale, changes in latent heating profile can impact mesoscale circulations (Fan et al., 2012; Zang et al., 2023).

This paper presents results from a 3D cloud-resolving model (CRM; i.e., using a few km grid spacing) inter-comparison project (MIP), conducted under the auspices of GEWEX (Global Energy and Water Exchanges) program, that utilizes the Radiative-Convective-Equilibrium MIP (RCEMIP) framework with a focus on ACI (RCEMIP-ACI). RCE represents the equilibrium state the atmosphere would attain in the absence of lateral

energy transport (Held et al., 1993; Jakob et al., 2019; Manabe & Wetherald, 1967). This idealized setup provides a reasonable approximation of the collective large-scale tropical (characterized by net precipitation) and subtropical (characterized by net evaporation and radiative cooling) regimes of the atmosphere (Dagan & Stier, 2020; Jakob et al., 2019). It is important to note that, in the real atmosphere, circulation and energy exchanges between the subtropics and deep tropics play a crucial role in maintaining conditions close to RCE (Dagan, Stier, Dingley, & Williams, 2022; Jakob et al., 2019).

This MIP follows a previous, non-aerosol-focused MIP known as RCEMIP (Wing et al., 2018, 2020). The RCEMIP protocol eliminates rotation, maintains uniform solar insolation, and prescribes horizontally uniform sea surface temperatures (SST). Despite these simplifications, RCE simulations adequately approximate the collective tropical-subtropical conditions due to minimal Coriolis forces and the high heat capacity of the oceans. The RCE framework has been used for decades to study convection (Held et al., 1993; Manabe & Wetherald, 1967; Muller & Held, 2012; Silvers et al., 2023; Stephens et al., 2008; Tompkins & Craig, 1998; Wing et al., 2020) and, specifically, the role of aerosol-radiation interactions in convective development and aggregation (Dagan & Eytan, 2024; Dingley et al., 2021). However, despite a few recent studies (van den Heever et al., 2011; Beydoun & Hoose, 2019; Dagan, 2024; Lorian & Dagan, 2024), it remains underutilized for studying ACI.

The goal of this RCEMIP-ACI is to compare cloud responses to aerosol perturbations across a range of environmental SST conditions, focusing specifically on the simplified case of RCE. This contrasts with a previous MIP, which concentrated on the transient response (Marinescu et al., 2021). While the equilibrium response may overestimate the effects of aerosols on environmental conditions (Dagan, Stier, Spill, et al., 2022; Spill et al., 2021), this setup allows us to explore the sensitivity of RCE climate, cloud feedbacks (Dagan, 2022a), precipitation efficiency (Lutsko & Cronin, 2018), and convective aggregation (Beydoun & Hoose, 2019; Muller & Held, 2012) to the baseline state of assumed aerosol or cloud droplet concentrations. Furthermore, given the recent rise in RCE studies (Wing et al., 2020), it is important to assess the sensitivity of their results to the assumed aerosol concentrations. In addition, focusing on the equilibrium state—rather than the transient response—is more relevant for examining how clouds, large-scale circulation, and climate respond to persistent aerosol sources, as opposed to short-lived perturbations. Such persistent sources include industrial emissions, shipping corridors, and potential future marine cloud brightening activities (Christensen et al., 2022; Diamond et al., 2020; Latham et al., 2012). This paper presents the intercomparison protocol, the data set and initial analysis.

2. RCEMIP-ACI Simulations

A total of 11 modeling teams participated in RCEMIP-ACI (see Table 1). Each of the teams run the cloud-resolving model (CRM) simulations introduced in RCEMIP (Wing et al., 2018) under three different levels of CCN or CDNC (for simplicity, both will be denoted here as N_a). Models using CCN perturbations prescribed their near-surface concentrations at 1% supersaturation to 20, 200, and 2,000 cm^{-3}. Models using CDNC perturbation set the concentration to 20% less than the CCN perturbations mentioned above, that is, 16, 160, and 1,600 cm^{-3}, to account for the fact that not all CCN will be activated. The aerosol concentrations are prescribed as vertically uniform in most models, except in RAMS, where they are assumed to decrease with height in proportion to air density, and in WRF_progSS, which applies the Twomey activation formula (Twomey, 1959) with adjusted coefficients to yield CDNC values of 16, 160, and 1,600 cm^{-3} at 1% supersaturation in the different cases.

Aerosol-radiation interactions are not included in this MIP. Seven of the models account for a direct interaction between microphysics and radiation (i.e., including the Twomey effect (Twomey, 1974) for both liquid and ice; see Table 3). The large N_a range considered here is useful for establishing physical understanding. In addition, we note that observational-based studies (e.g., Choudhury and Tesche (2023)) show the plausibility of the N_a range considered here. Only three of the models—RAMS, SAM_P3ice and WRF_progSS—do not employ saturation adjustment (i.e., immediately restoring air to saturation) for condensation and evaporation and hence can potentially better represent the relevant physics for warm phase invigoration (Koren et al., 2014).

Four model configurations are included in this study (Table 2), following the setup of Wing et al. (2018). As the modeling setup was detailed in Wing et al. (2018), we will only provide a brief overview here.

The small-domain simulations (RCE_small) use a domain size of approximately 100×100 km^2 (see Table 2). These smaller domains minimize the effects of convective self-aggregation (Muller & Held, 2012; Wing

Table 1
List of Participating Models

Model abbreviation	Model name/version	Main references
DALES	Dutch Atmospheric Large-Eddy Simulation model v4.4.2	Heus et al. (2010)
MicroHH	MicroHH 2.0	Van Heerwaarden et al. (2017)
MESONH	Meso-NH v5-6	Lac et al. (2018)
ICON	ICOsahedral Nonhydrostatic model v2.6.6	Zängl et al. (2015)
DAM	Das Atmosphaerische Modell	Romps (2008)
RAMS	Regional Atmospheric Modeling System v6.3.04	Cotton et al. (2003) and Saleeby and van den Heever (2013)
SAM_M2005	System for Atmospheric Modeling v6.11.8, Morrison et al. (2005) microphysics	Khairoutdinov and Randall (2003) and Morrison et al. (2005)
SAM_P3ice	System for Atmospheric Modeling v6.10.9 with modified P3 microphysics	Khairoutdinov and Randall (2003), Morrison and Milbrandt (2015), and Gasparini et al. (2025)
XSHiELD	XSHiELD	Harris et al. (2020)
WRF_IITM	Weather Research and Forecasting (WRF) model V3.9.1	Skamarock et al. (2008)
WRF_progSS	WRF V4.6.0, Morrison et al. (2005) with predicted droplet concentrations and prognostic supersaturation	Morrison et al. (2005) and Zhang et al. (2021)

Table 2
Simulation Configurations Included in the Model Intercomparison Project

Simulation type	Domain size	Grid spacing	Vertical levels
RCE_large	$\sim 6000 \times 400$ km^2	3 km	$\sim$74
RCE_small	$\sim 100 \times 100$ km^2	1 km	$\sim$74
RCE_small_les	$\sim 100 \times 100$ km^2	200 m	146
RCE_small_vert	$\sim 100 \times 100$ km^2	1 km	146

et al., 2018), making them suitable for studying local clouds and radiation impacts. Three grid configurations are considered for RCE_small:

1. RCE_small: grid with 1 km horizontal spacing and 74 vertical levels, as defined in Wing et al. (2018).
2. RCE_small_vert: Same horizontal grid spacing of 1 km but with approximately twice the vertical resolution (146 levels), to test sensitivity to vertical resolution.
3. RCE_small_les: Higher horizontal (200 m) and vertical (146 levels) resolution, simulating large eddy simulations (LES) for fine-scale processes.

In the analysis presented in this paper, we combine all three RCE_small domain simulations for simplicity. As a result, we include 14 different RCE_small simulation sets (see Table 3). Future work will explore the sensitivity of the aerosol response to both vertical and horizontal resolution. However, to provide an initial view of the resolution dependency of our results, in Text S1 in Supporting Information S1 we present the results separated by the simulation resolution, for the interested reader.

Additionally, large-domain simulations (RCE_large) use a domain size of approximately 6000 $\times$ 400 km^2 with a horizontal grid spacing of 3 km. These simulations capture convective self-aggregation (Muller & Held, 2012; Wing et al., 2018) and large-scale circulation formed by interactions between convective clusters and surrounding dry, subsiding regions (Dagan, 2024; Silvers et al., 2023). This large-domain setup is valuable for examining the role of clouds in large-scale phenomena.

Most models conducted the RCE_small and RCE_large simulations, while two models conducted the RCE_small_vert and RCE_small_les simulations (Table 3). For each configuration, each model conducted nine simulations under three different SSTs—295, 300, and 305K and three different N_a for each SST.

Other than that, we follow Wing et al. (2018): the concentration of CO_2 is fixed at pre-industrial level (280 ppm) and other trace gas concentrations are set identical to Wing et al. (2018). In addition, the solar insolation is set close to the tropical-mean value, by fixing the solar radiation at 551.58 W m^{-2}, with a zenith angle of 42.05° (Wing et al., 2018). A diurnal cycle is not considered here and we used the initial conditions, simulation length (100-day), and domain top for all configurations (33 km) as defined in Wing et al. (2018). The statistical analysis is based on the last 30-day of each simulation in which the simulations are close to RCE conditions. The output variables and their time frequency, provided by the different models, are listed in Tables S1–S4 in Supporting Information S1. WRF_progSS did not output the 2D vertical velocity at the 500 hPa level. Thus, we use here interpolated data from the 3D output. In addition, this model did not use the same vertical levels as defined in Wing et al. (2018) but instead used a different grid with the same number of vertical levels (74) and the same domain top (33 km).

Table 3
Simulation Configuration Conducted by Each Model

Model	RCE_large	RCE_small	RCE_small_les	RCE_small_vert	Twomey effect represented
DALES			✓	✓	✓
MicroHH		✓	✓	✓	✓
MESONH	✓	✓			
ICON	✓	✓			✓
DAM	✓	✓			
RAMS	✓	✓			✓
SAM_M2005	✓	✓			✓
SAM_P3ice	✓	✓			✓
XSHiELD	✓	✓			
WRF_IITM	✓	✓			
WRF_progSS	✓	✓			✓
Number of models	9	10	2	2	7

DALES was inadvertently run with a homogeneous setting for the surface scheme, where surface fluxes are calculated from the mean wind instead of the local wind. This decreases the surface fluxes and results in a lower liquid water path. However, we expect this setting not to directly affect the response to perturbing the cloud droplet number concentration.

To compactly represent model responses across the large data set presented here (207 simulations in total), many of the analyses below focus on the difference between the most polluted and the cleanest cases, divided by two. This provides an estimate of the response to an order-of-magnitude increase in aerosol concentration. The corresponding responses based on the two other available aerosol concentration contrasts are presented in the Supporting Information S1. In most cases, the responses are approximately linear and do not strongly depend on which aerosol concentration difference is used for their calculation. In addition, where appropriate, we average the results across models for a given simulation configuration and present the interquartile range to convey the spread and variability among the different models.

3. Results and Conclusions

3.1. Aerosol Impact on Domain Mean Properties

We start by examining the impact of aerosol on domain and time mean properties such as top of atmosphere (TOA) outgoing shortwave radiation (OSR), TOA outgoing longwave radiation (OLR), liquid water path (LWP; vertically integrated liquid water content), ice water path (IWP; vertically integrated ice content), and surface precipitation (P; Figure 1). Figure 1a demonstrates that $\frac{dOSR_{SST_i}}{d \log N_a}$ tends to be positive in most models and SSTs, representing an increase in shortwave reflection at TOA with an increase in aerosol loading. However, some models demonstrate a negative $\frac{dOSR_{SST_i}}{d \log N_a}$ for some of the SSTs, and the interquartile range also covers negative values in many of the cases.

Similarly, the LWP response (Figure 1c) also tends to be positive on average (especially in the RCE_large simulations) but small and noisy (i.e., negative in some of the models). On the other hand, the OLR, IWP, and P response (Figures 1b, 1d, and 1e) demonstrates no consistent trend with N_a across models and SSTs. This weak radiative sensitivity to aerosol loading in RCE simulations is consistent with a previous single-model-based study (Dagan et al., 2023) and is argued to be driven by the fact that RCE simulations mostly produce deep convective clouds (C. Stauffer & Wing, 2023; C. L. Stauffer & Wing, 2024), which are less sensitive to aerosol loading than shallow clouds (Wall et al., 2022).

Further examination of the response of vertical profiles of liquid water in the clouds (q_c) to an increase in N_a (Figures 2a and 2b) suggests that in all model configurations and SSTs examined here, an increase in N_a acts to increase q_c in the lower to mid-troposphere (at the layer between 1 and 5–6 km). This trend is in agreement with previous studies (Abbott & Cronin, 2021; Albrecht, 1989; Dagan et al., 2023; Lorian & Dagan, 2024; Marinescu et al., 2021) and can be explained by warm rain suppression due to an increase in N_a at the lower troposphere (Figures 2c and 2d). The positive q_c response at the mid-troposphere is partially counteracted in the boundary layer (at roughly the lower 1 km), which results in a weak total LWP response (Figure 1c).

The increase in q_c in the mid-troposphere provides additional cloud water for detrainment aloft, leading to higher water vapor content (q_v; Figures 3a and 3b). This response is consistent across all model configurations and SSTs, aligning with previous findings from single-model simulations (Abbott & Cronin, 2021; Dagan, 2024; Lorian & Dagan, 2024), thereby demonstrating its robustness.

Furthermore, consistent with earlier single-model RCE simulations (Abbott & Cronin, 2021; Dagan, 2024; Lorian & Dagan, 2024), our multi-model mean data set also shows that the mid-tropospheric increase in q_v is accompanied by a rise in air temperatures, peaking in the upper troposphere (Figures 3c and 3d). This pattern can be attributed to reduced entrainment cooling effect with increased q_v, which relatively warms convective air (Abbott & Cronin, 2021; Singh & O'Gorman, 2013) and affects the domain mean temperature profile (Sobel et al., 2001). The resulting upper-tropospheric warming affects atmospheric static stability (Lorian & Dagan, 2024) and is thus expected to influence large-scale circulation (see Section 3.4 below; (Silvers et al., 2023)). We note that in Figure 3, the intermodel spread is larger in the RCE_large compared with the RCE_small simulations, which we speculate could be driven by differences in the baseline level of convective organization.
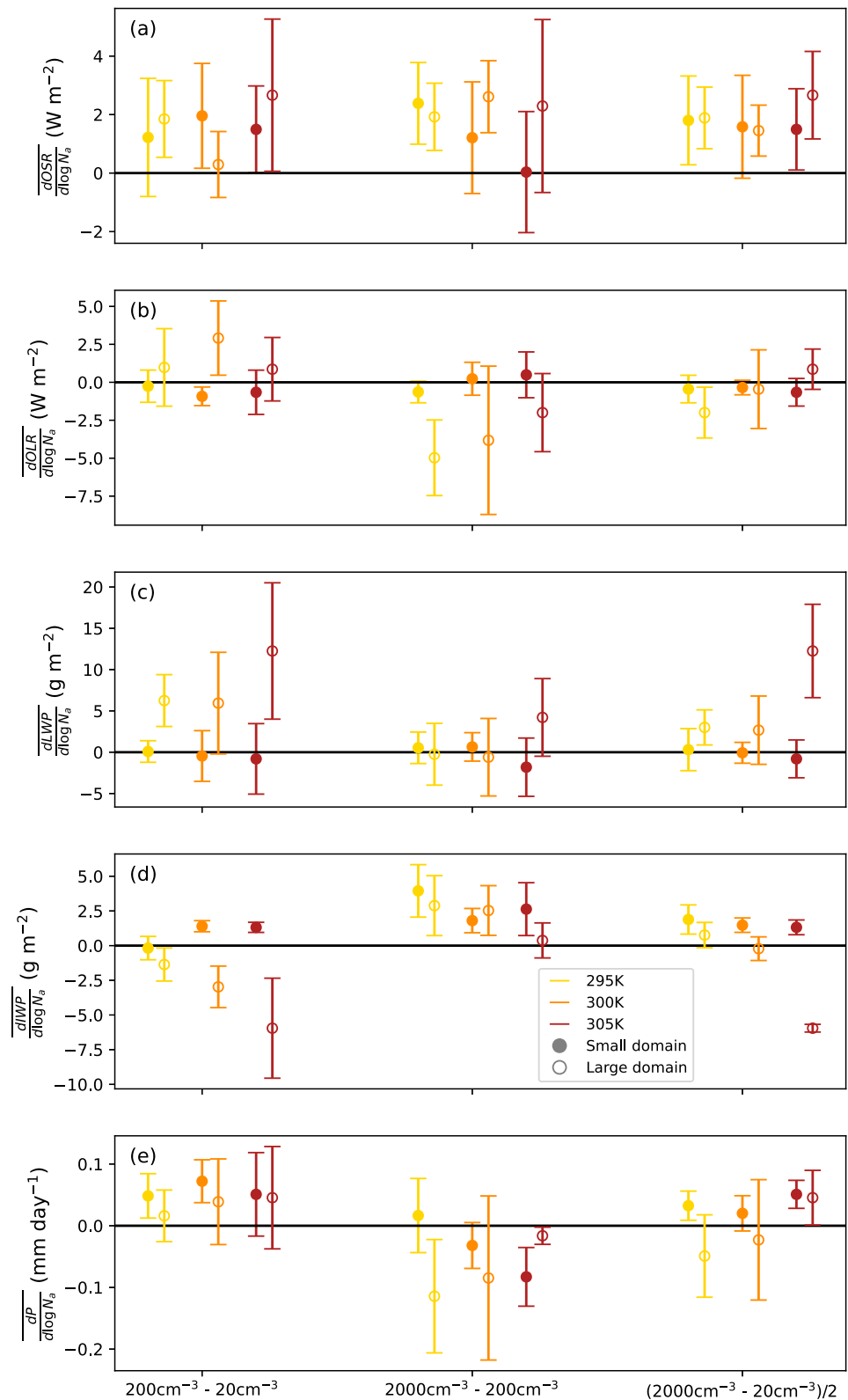
Figure 1. Domain and time mean N_a-driven response of: (a) top of atmosphere (TOA) outgoing shortwave radiation (OSR), (b) TOA outgoing longwave radiation (OLR), (c) liquid water path (LWP), (d) ice water path (IWP), and (e) surface precipitation (P), for the different aerosol contrasts and sea surface temperatures (the different colors). Error bars represent the interquartile range of the different models.
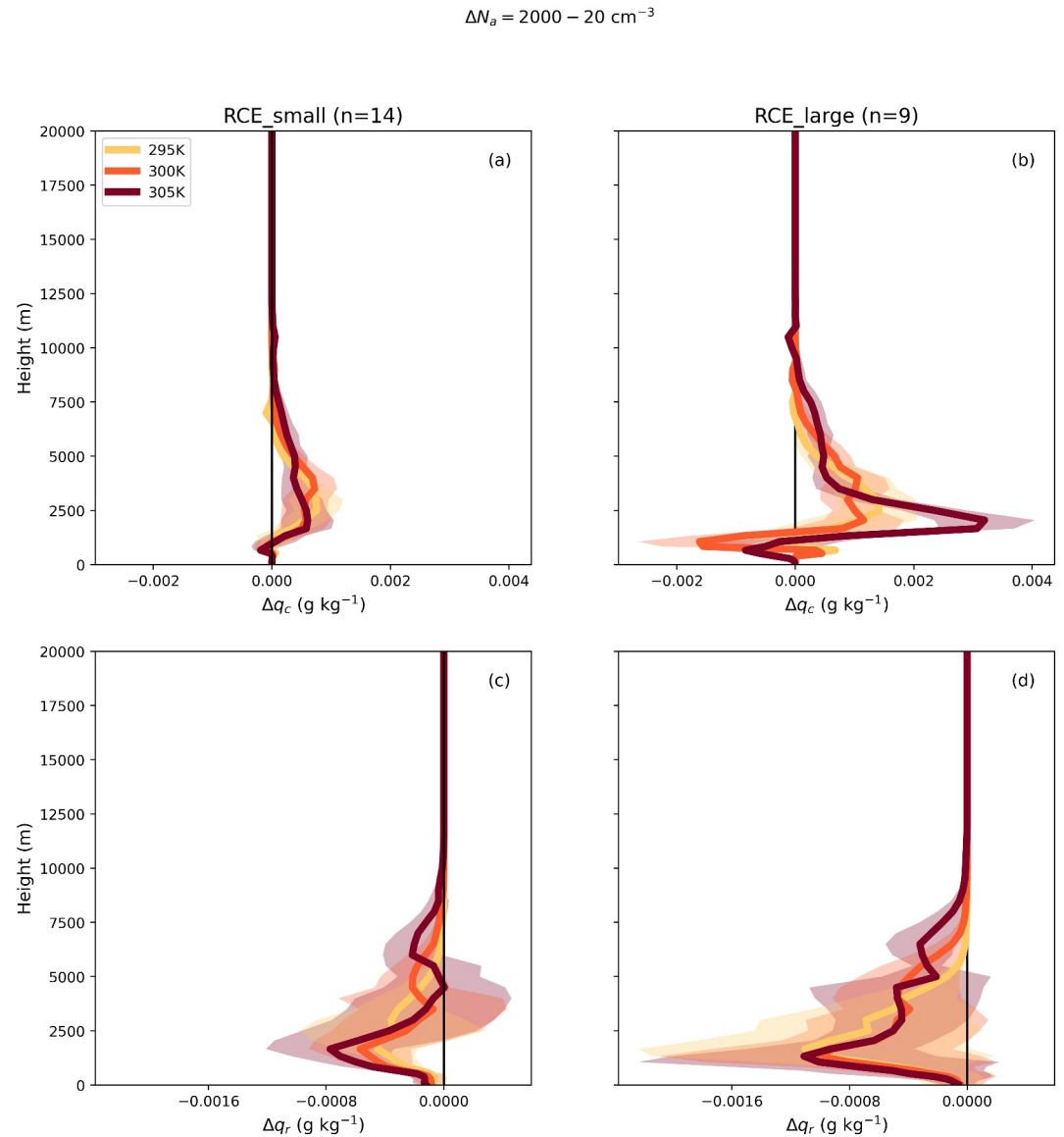
Figure 2. Domain and time mean N_a-driven multi-model mean response of the vertical profile of: (a, b) cloud liquid water content (q_c), and (c, d) rain water content (q_r), for the different model configurations and sea surface temperatures (the different colors). Shaded areas represent the interquartile range of the different models. This figure is based on the difference between the most polluted (2000 cm^{-3}) and cleanest (20 cm^{-3}) simulations in each model, divided by two to represent the response to an order-of-magnitude change in aerosol concentration. The responses based on the two other available aerosol contrasts (200–20 and 2,000–200 cm^{-3}) are presented in Figures S1 and S2 in Supporting Information S1, while the baseline vertical profiles of q_c and q_r are shown in Figure S3 in Supporting Information S1.

In addition, an aerosol-driven increase in upper-tropospheric static stability has previously been shown to reduce anvil cloud coverage through a mechanism analogous to the stability iris effect (Bony et al., 2016; Lorian & Dagan, 2024). In this mechanism, increased static stability weakens the clear-sky subsidence required to balance radiative cooling. This leads to a reduction in radiatively driven divergence in the upper troposphere, which in turn decreases detrainment and, consequently, anvil cloud fraction. This response is illustrated in Figure 4, which shows a consistent reduction in upper-tropospheric cloud fraction with increasing aerosol loading, across a range of SSTs, domain configurations, and models.
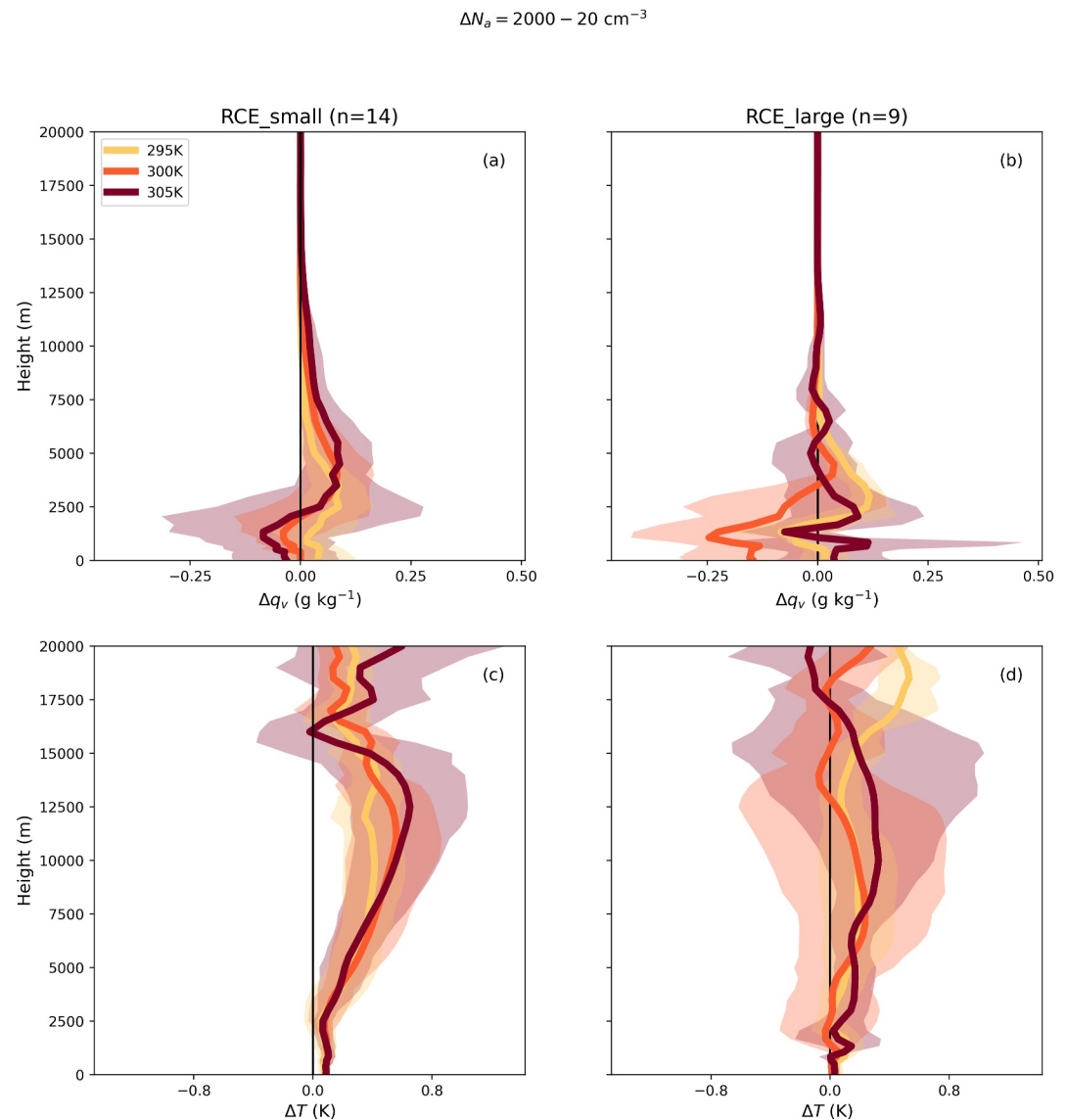
Figure 3. Domain and time mean N_a-driven multi-model mean response of the vertical profile of: (a, b) water vapor content (q_v), and (c, d) air temperature (T), for the different model configurations and sea surface temperatures (the different colors). Shaded areas represent the interquartile range of the different models. This figure is based on the difference between the most polluted (2000 cm^{-3}) and cleanest (20 cm^{-3}) simulations in each model, divided by two to represent the response to an order-of-magnitude change in aerosol concentration. The responses based on the two other available aerosol contrasts (200–20 and 2,000–200 cm^{-3}) are presented in Figures S4 and S5 in Supporting Information S1, while the baseline vertical profiles of q_v and T are shown in Figure S6 in Supporting Information S1.

3.2. Aerosol Impact on Convective Intensity

As the influence of aerosols on convection remains a topic of debate (Williams et al., 2002; Rosenfeld et al., 2008; A. C. Varble et al., 2023; Romps et al., 2023), it is valuable to examine how convection intensity responds to aerosol concentration in our multi-model simulations. To investigate this, we analyze high updraft velocities in the different models ($w_{99.999}$), which represent the 99.999th percentile of vertical velocity at the 500 hPa level over time and space. This metric approximates the maximum vertical velocity while being less sensitive to rare, extreme values (Figures 5 and 6). The results presented here are not sensitive to the exact high percentile chosen, as demonstrated in Figures S10–S15 in Supporting Information S1, which show similar responses for the 99.9th, 99.99th, and 99.9999th percentiles.
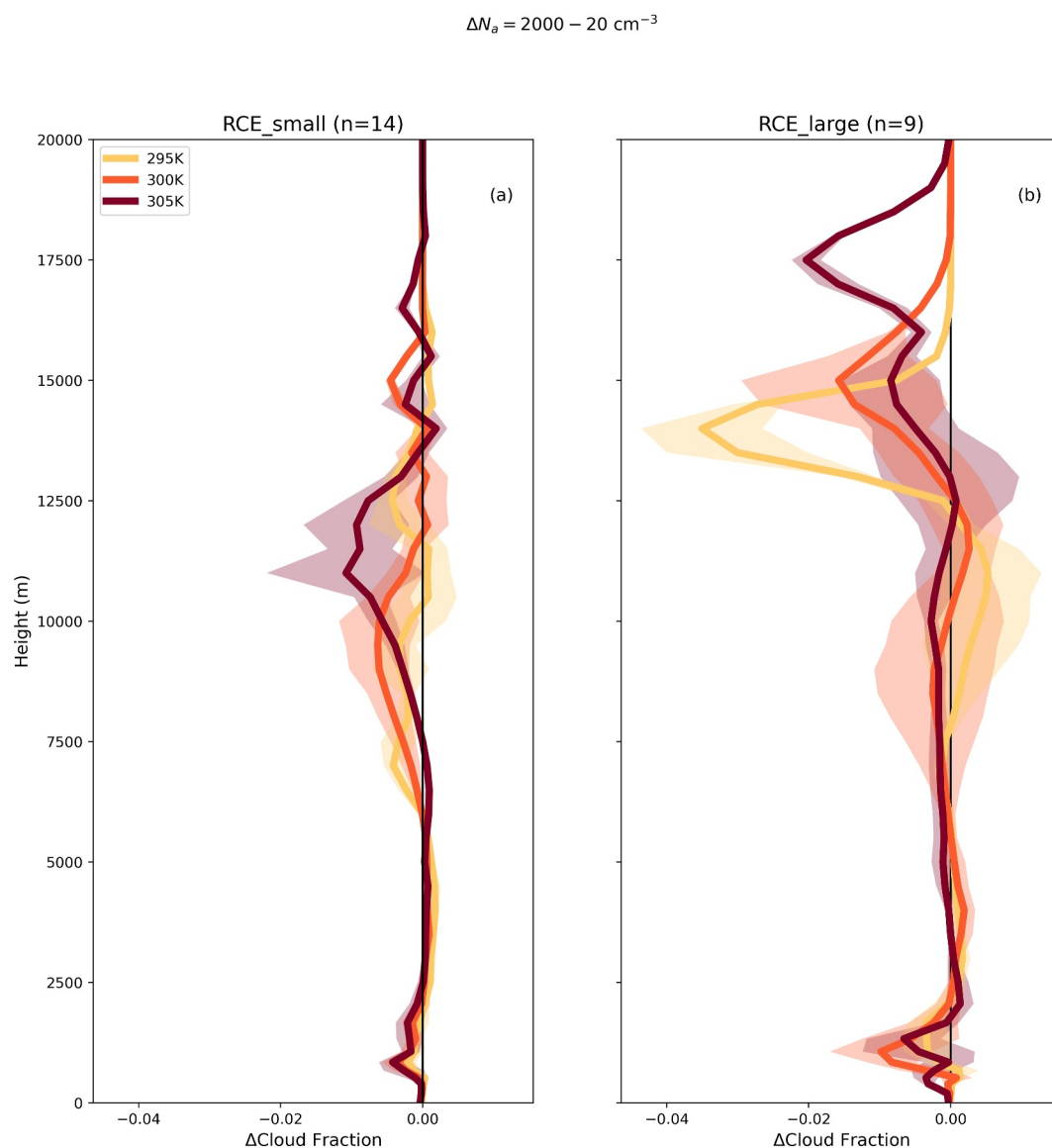
Figure 4. Domain and time mean N_a-driven multi-model mean response of the cloud fraction for the different model configurations and sea surface temperatures (the different colors). Shaded areas represent the interquartile range of the different models. This figure is based on the difference between the most polluted (2000 cm^{-3}) and cleanest (20 cm^{-3}) simulations in each model, divided by two to represent the response to an order-of-magnitude change in aerosol concentration. The responses based on the two other available aerosol contrasts (200–20 and 2,000–200 cm^{-3}) are presented in Figures S7 and S8 in Supporting Information S1, while the baseline vertical profiles of the cloud fraction are shown in Figure S9 in Supporting Information S1.

Figure 5a illustrates that convection intensity varies significantly among models in the RCE_small simulations, with values spanning a factor of seven (ranging from 3 to 21 m s^{-1}). The response of convection intensity to aerosol concentration (Figure 5b) indicates that, within this modeling framework, on average, aerosols appear to slightly invigorate convection intensity. However, the mean response is very small (<0.2 m s^{-1} for all SSTs) and not consistent across models. Specifically, only three of the 14 models demonstrate a positive response for all SSTs (WRF_progSS, which uses fully prognostic supersaturation, DALES RCE_small_vert and SAM_P3ice).

Similarly, in RCE_large simulations, the magnitude of w$_{99.999}$ varies significantly between the models, exhibiting a multi-model range spanning a factor of four (Figure 6a; between 4 and 16 m s^{-1}). Once again, the response of w$_{99.999}$ to aerosol concentration (Figure 6b) does not reveal a consistent trend across the models or SSTs.
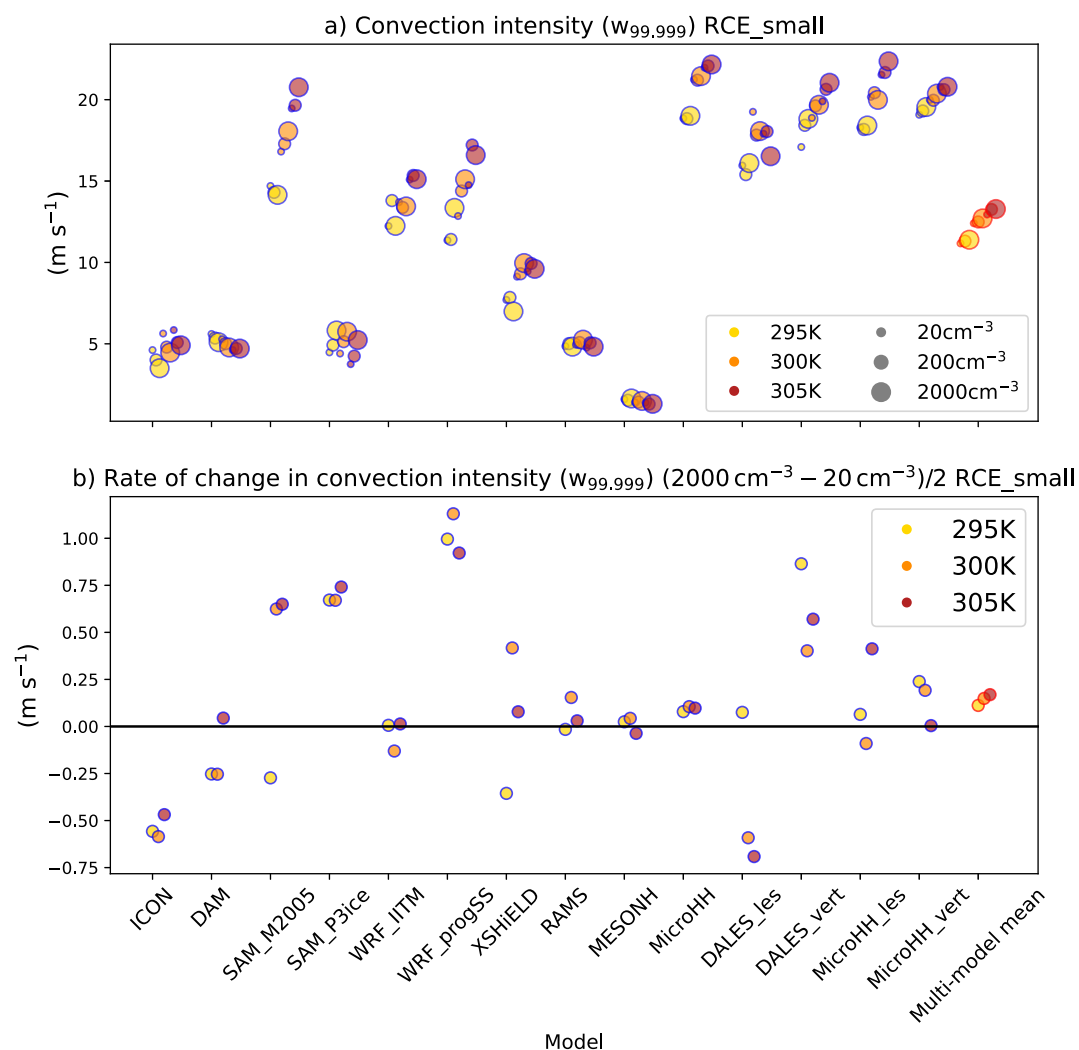
Figure 5. Convection intensity, defined as the 99.999th percentile of the vertical velocity ($w_{99,999}$) at the 500 hPa level (a), and the rate of change in $w_{99,999}$ with aerosol concentration (b) in RCE_small simulations in all models. Markers circled in red on the right side of each panel indicate the multi-model mean. This figure is based on the difference between the most polluted (2000 cm^{-3}) and cleanest (20 cm^{-3}) simulations in each model, divided by two to represent the response to an order-of-magnitude change in aerosol concentration. The responses based on the two other available aerosol contrasts (200–20 and 2,000–200 cm^{-3}) are presented in Figure S16 in Supporting Information S1.

These results suggest that aerosols do not consistently invigorate convection across the multi-model RCE simulations presented here in keeping with the previous MIP results (Marinescu et al., 2021). This conclusion holds regardless of the vertical velocity percentile defined as strong convection (Figures S10–S15 in Supporting Information S1). However, we acknowledge that the definition used here for invigoration is pretty narrow, and in future work, we plan to investigate the sensitivity of vertical velocity to aerosol loading at different vertical levels and stages of cloud development (Marinescu et al., 2021). It is also important to note that only three of the models used in this study do not employ saturation adjustments (WRF_progSS, SAM_P3ice and RAMS). Hence, the representation of the "warm-phase" invigoration mechanism (Fan et al., 2018; Igel & van den Heever, 2021; Koren et al., 2014; Sheffield et al., 2015) might be partially lacking. These models that do not employ saturation adjustments do demonstrate a slight increase in vertical velocity with an increase in aerosol concentration in RCE_small but not in RCE_large. Additionally, a non-spatially-uniform aerosol perturbation (in contrast to the uniform increase in aerosol concentration examined here) could have a stronger impact on large-scale conditions and, consequently, invigorate convection (Abbott & Cronin, 2021). This possibility will also be explored in future work.
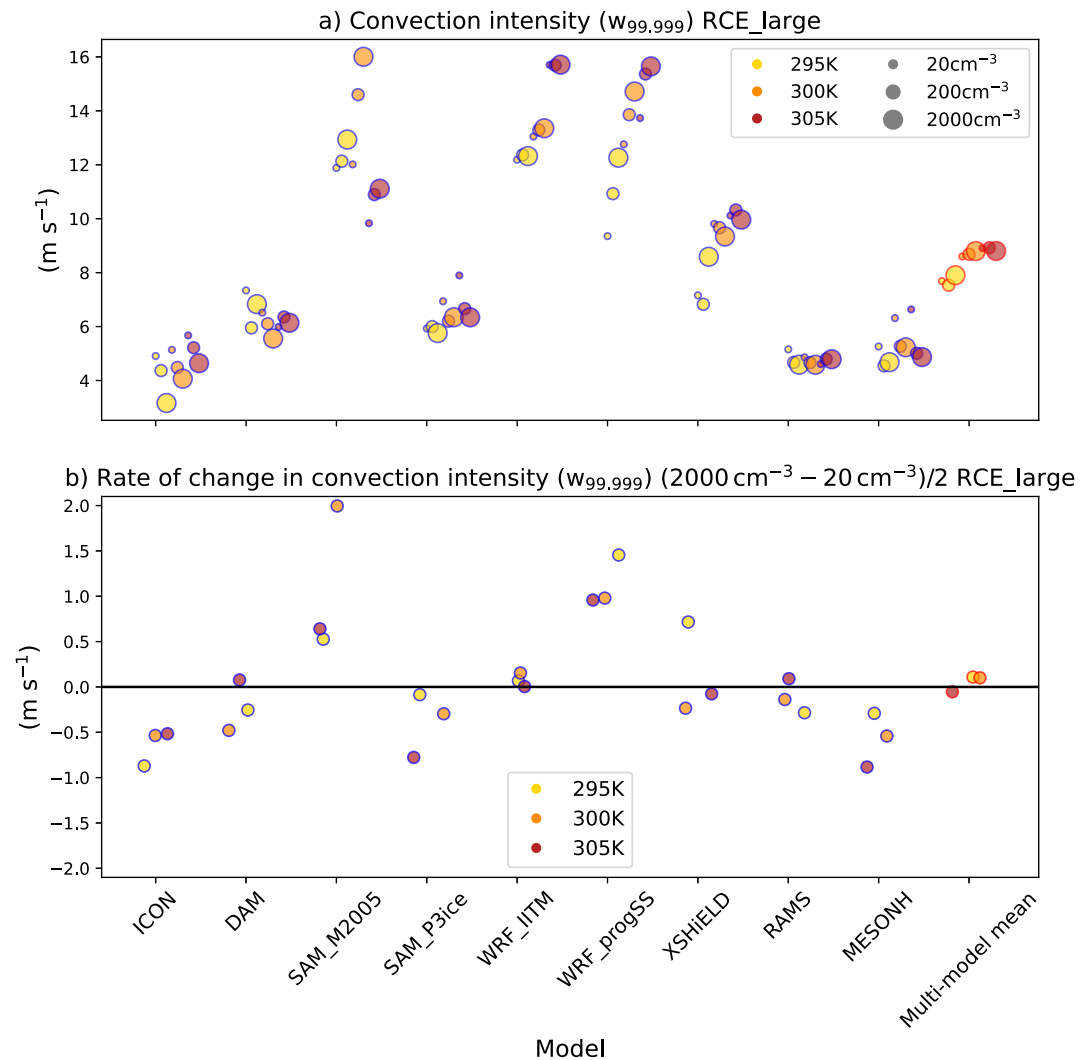
Figure 6. Convection intensity, defined as the 99.999th percentile of the vertical velocity ($w_{99.999}$) at the 500 hPa level (a), and the rate of change in $w_{99.999}$ with aerosol concentration (b) in RCE_large simulations in all models. Markers circled in red on the right side of each panel indicate the multi-model mean. This figure is based on the difference between the most polluted ($2000 \, cm^{-3}$) and cleanest ($20 \, cm^{-3}$) simulations in each model, divided by two to represent the response to an order-of-magnitude change in aerosol concentration. The responses based on the two other available aerosol contrasts (200–20 and 2,000–200 cm^{-3}) are presented in Figure S17 in Supporting Information S1.

3.3. Aerosol Impact on Convective Aggregation

It is widely appreciated that convection tends to aggregate in large-domain RCE simulations (Muller & Held, 2012; Wing et al., 2020). Figure 7 presents two organization metrics for all RCE_large simulations—the organization index (i_{org}) and subsidence fraction (f_{SB}) (Tompkins & Semie, 2017; Wing et al., 2020). Although there are many organization indices (see Biagioli and Tompkins (2023) for a review), i_{org} is a widely used clustering metric that evaluates how the distribution of deep convective entities compares to a random distribution by analyzing nearest neighbor distances (Tompkins & Semie, 2017; Weger et al., 1992). f_{SB} represents the fraction of the domain area where the daily average large-scale vertical velocity at 500 hPa is downward. This vertical velocity is first averaged over a day in time and over spatial blocks of approximately $100 \times 100 \, km^2$. The more aggregated the system, the more spatially concentrated the updrafts and the more widespread the subsidence, hence f_{SB} increases with the level of aggregation. These values are defined and calculated as in Wing et al. (2020). Values above 0.5 for both metrics represent an aggregated state (Tompkins & Semie, 2017; Wing et al., 2020).
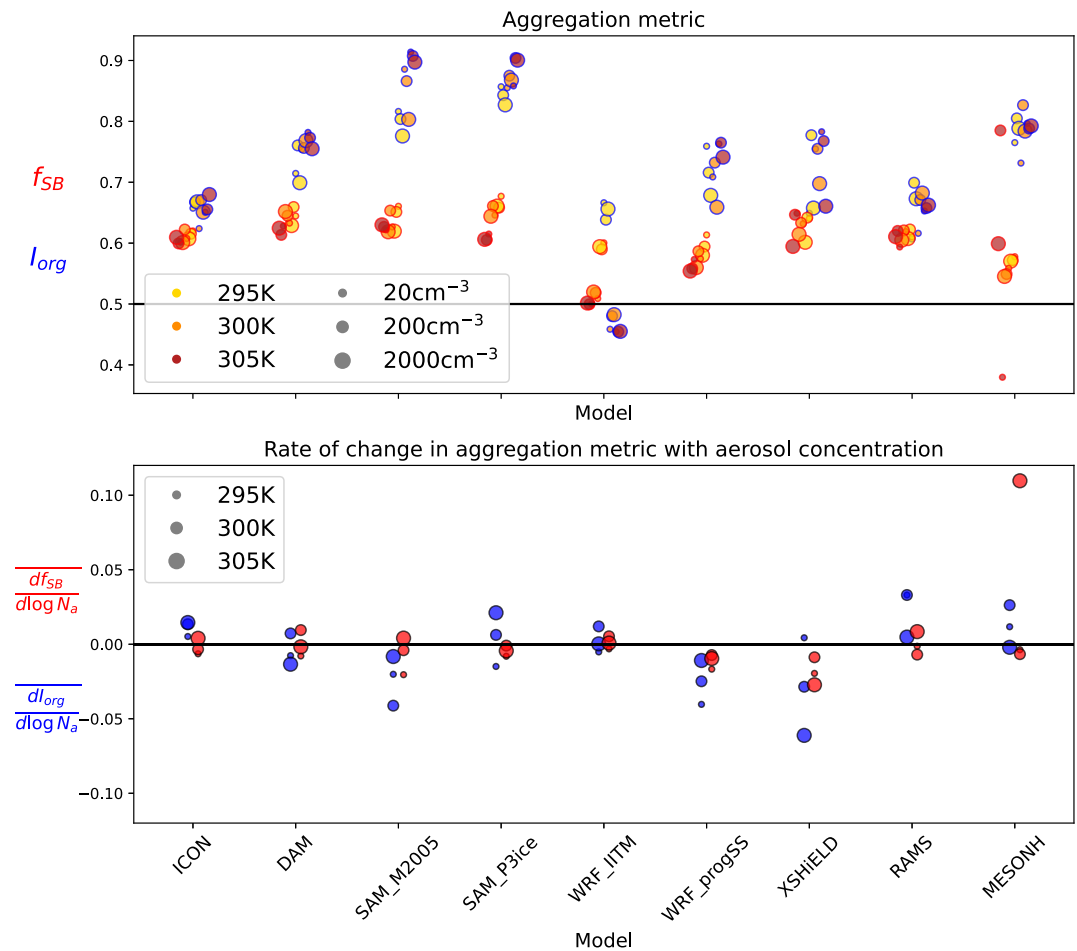
Figure 7. Degree of aggregation (a), and the rate of change in the degree of aggregation with aerosol concentration (b) in RCE_large simulations for all models. The degree of aggregation is based on subsidence fraction (f_{SB}; red circles), and i_{org} (blue circles), calculated for the last 30-day of the simulations.

Figure 7a demonstrates that, other than many of the WRF_IITM simulations and one simulation conducted with MESONH, all large-domain simulations are aggregated.

Examining the change in the aggregation metrics with an increase in N_a for each SST (Figure 7b) reveals no consistent trend. Most models exhibit a mean change close to zero (within ±0.05) for all SSTs, with only two models showing changes outside this range for a single SST and one aggregation matrix. Specifically, for XSHiELD, $\frac{di_{org}}{d \log N_a}$ at an SST of 305 K is approximately −0.06, while for MESONH, $\frac{df_{SB}}{d \log N_a}$ at an SST of 305 K is roughly 0.1.

This lack of consistent aggregation sensitivity to aerosol concentration places the results of the previous single-model RCE study (Beydoun & Hoose, 2019)—which found a reduction in convective aggregation with increasing aerosol concentration—into a broader context, demonstrating that the aerosol effect on aggregation is strongly model-dependent. Why aggregation is insensitive in a consistent way to aerosols in our multi-model ensemble deserves a separate study. However, as cloud-longwave radiation interactions were shown to be the biggest drivers of self-aggregation in RCEMIP (Pope et al., 2023), we can speculate that the lack of consistent aggregation sensitivity to aerosol concentration is driven by a non-consistent change in OLR and in IWP (Figure 1), which strongly impacts longwave radiation.
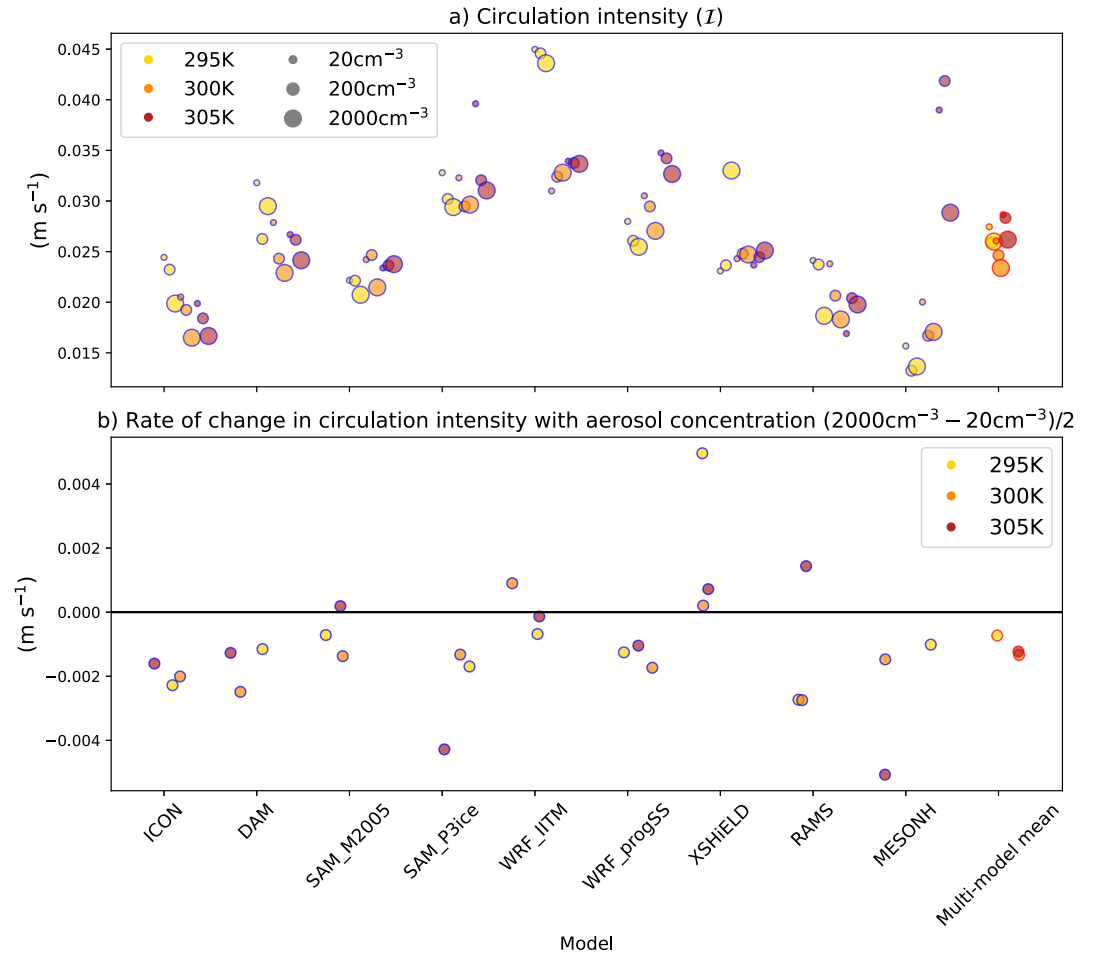
Figure 8. Circulations intensity (a; $\mathcal{I}$), and the rate of change in $\mathcal{I}$ with aerosol concentration (b) for RCE_large simulations in all models. Markers circled in red on the right side of each panel indicate the multi-model mean. This figure is based on the difference between the most polluted ($2000\,\text{cm}^{-3}$) and cleanest ($20\,\text{cm}^{-3}$) simulations in each model, divided by two to represent the response to an order-of-magnitude change in aerosol concentration. The responses based on the two other available aerosol contrasts (200–20 and 2,000–200 cm^{-3}) are presented in Figure S18 in Supporting Information S1.

3.4. Aerosol Impact on Large-Scale Circulation Intensity

As noted in previous studies (Dagan, 2024; Silvers et al., 2023), RCE_large simulations exhibit the formation of a large-scale circulation between convective clusters and the surrounding dry regions. This type of circulation develops even under spatially uniform SST conditions and is therefore distinct from more realistic large-scale circulations—such as the Hadley or Walker cells—which are driven by horizontal SST gradients.

For evaluating the strength of the overturning tropical circulation formed in these RCE_large simulations, we follow previous studies (Bony et al., 2013; Dagan, 2024; Medeiros et al., 2015; Silvers et al., 2023) and examine $\mathcal{I}$, which is defined as follows:

$$\mathcal{I} = w^{\uparrow} - w^{\downarrow} \tag{1}$$

In Equation 1, $w^{\uparrow}$ represents the time- and domain-mean upward vertical velocity, and $w^{\downarrow}$ represents the time- and domain-mean downward vertical velocity at the 500 hPa level. To examine the large-scale circulation, we first coarsen w to a grid with blocks of $96 \times 96\,\text{km}^2$, as done, for example, in Silvers et al. (2023). The multi-model range of $\mathcal{I}$ is shown to be approximately a factor of three (Figure 8a), again highlighting that even in RCE simulations, models exhibit a high degree of variability (Silvers et al., 2023).

Examining the impact of increased N_a concentration on large-scale circulation intensity (Figure 8b) shows that, in most models, it tends to reduce circulation intensity. Specifically, this reduction occurs in 8, 7, and 6 out of 9 models for SSTs of 295, 300, and 305 K, respectively. Consequently, the multi-model mean exhibits a reduction of approximately 0.001 m s^{-1}, representing a weak but SST-consistent decrease of about 5% for an order of magnitude increase in N_a.

This general weakening of large-scale circulation intensity with increasing aerosol concentration contrasts with findings from a previous single-model RCE study (Dagan, 2024). However, it is important to note that in Dagan (2024), w was not coarsened to a grid with blocks of 96 × 96 km^2, as we did here. This methodological difference is likely to explain the contrasting conclusions between our results and those of Dagan (2024). (In the multi-model mean, the change in $\mathcal{I}$ is positive when calculated based on the grid-box vertical velocity for all SSTs, but becomes negative when calculated using the large-scale (96 × 96 km^2) vertical velocity).

Additionally, recent studies have shown that aerosols tend to intensify large-scale circulation intensity in the presence of a more realistic, persistent, and geographically oriented tropical overturning circulation (e.g., a mock Walker setup (Dagan, 2022b; Dagan et al., 2023)). However, the proposed mechanism for this intensification involves interactions between shallow cloud and deep cloud regimes. Since RCE simulations generally lack a shallow cloud regime (C. Stauffer & Wing, 2023; C. L. Stauffer & Wing, 2024; Wing et al., 2020), the dominant mechanism in our simulations must be different.

For a better understanding of the causes of the weak decrease in large-scale circulation intensity with aerosol concentration in our simulations, we adopt the weak temperature gradient approximation (Sobel et al., 2001). Based on this theoretical approximation, in the tropics, radiative cooling in the clear-sky free troposphere is balanced by warming associated with adiabatic subsiding motions. Thus, the free troposphere clear-sky energy budget can be formulated as follows:

$$Q_r = -S\omega_d \qquad (2)$$

where Q_r is the radiative cooling rate, ω_d is the clear sky vertical velocity, and S is the static-stability defined as:

$$S = -\frac{T}{\theta}\frac{\partial\theta}{\partial p} \qquad (3)$$

where T is the air temperature, θ is the potential temperature and p is the pressure.

Based on this theoretical argument, changes in large-scale circulation intensity (dominated by ω_d) can be driven by either changes in radiative cooling (Q_r) or static stability (S). While previous work has shown considerable variability in the RCEMIP archive regarding the relevant variables in Equation 2 (Silvers et al., 2023), the radiative-subsidence balance (Equation 2) remains a useful framework for examining the causes of changes in circulation intensity.

Therefore, in Figure 9, we present the aerosol-driven change in S (Figure 9a) and Q_r (Figure 9b), versus the change in $\mathcal{I}$, for all RCE_large simulations. These quantities are evaluated at the 500 hPa level. This figure demonstrates a general increase in S with aerosol concentration, consistent in the multi-model mean over all SSTs (Figure 9a; see also Figure S19 in Supporting Information S1), alongside a minimal and non-SST-consistent change in Q_r (Figure 9b; see also Figure S19 in Supporting Information S1). In addition, Figure 9 demonstrates a negative (−0.34) and statistically significant (at a p-value level of 0.1) correlation between the change in S and the change in $\mathcal{I}$, while a less negative (−0.15) and not statistically significant correlation between the change in Q_r and the change in $\mathcal{I}$. Based on these results, we conclude that the main driver for the reduction in large-scale circulation strength (Figure 8b) is the increase in S, which aligns with the upper tropospheric warming observed under high aerosol loading (Figure 3).

4. Summary

This study explores aerosol-cloud interactions (ACI) using a multimodel ensemble of radiative-convective equilibrium (RCE) simulations. The analysis examines how aerosol microphysical perturbations affect cloud properties, thermodynamic variables, and large-scale atmospheric circulation under equilibrium conditions
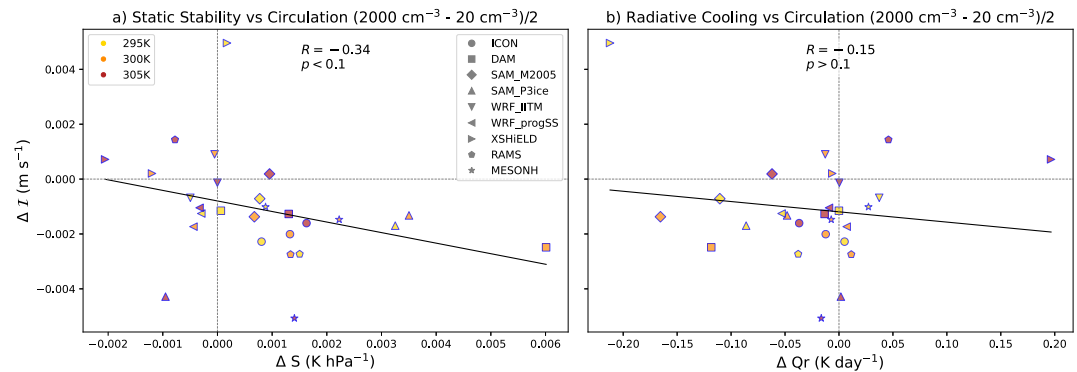
Figure 9. Aerosol-driven change in static stability (a; S) and radiative cooling (b; Q_r) versus the change in circulation intensity (I) for the different models and SSTs. These quantities are evaluated at the 500 hPa level and presented for RCE_large simulations in all models. This figure is based on the difference between the most polluted (2000 cm^{-3}) and cleanest (20 cm^{-3}) simulations in each model, divided by two to represent the response to an order-of-magnitude change in aerosol concentration. The responses based on the two other available aerosol contrasts (200–20 and 2,000–200 cm^{-3}) are presented in Figure S20 in Supporting Information S1.

(as opposed to transient simulations (Dagan, Stier, Spill, et al., 2022; Marinescu et al., 2021)). The data set consists of simulations from 11 cloud-resolving models with varying aerosol concentrations, domain configurations, and sea surface temperatures, providing a robust foundation for analysis. While the aerosol perturbation is represented somewhat differently across models (e.g., as changes in CCN vs. CDNC), the goal of this study is to investigate how aerosol perturbations affect cloud and circulation characteristics within each model. The aim is not to enforce cross-model consistency in aerosol–cloud microphysics, but rather to explore the model-specific responses under a common experimental framework. However, we acknowledge that the differences in CCN/CDNC representation between models could be one of the causes of the differences in the aerosol effects demonstrated here.

The findings reveal some consistent responses across the models, including the suppression of warm rain formation by aerosols, which enhances mid-tropospheric cloud water content and humidity. This increased humidity reduces entrainment cooling, warms the upper troposphere, and increases atmospheric static stability. We note that these findings are robust to the absence or presence of convective self-aggregation, as they are demonstrated in both the RCE_small and RCE_large simulations. Despite these commonalities, the study also highlights variability in the cloud radiative responses. Top-of-atmosphere shortwave and longwave radiation responses to aerosols differ significantly among models, reflecting uncertainties in aerosol-cloud interactions and the manner in which these interactions are represented within numerical models.

Interestingly, aerosols are not consistently found to affect convective self-organization or invigorate convection. However, they generally reduce the intensity of large-scale circulation, likely due to the increased static stability. The preliminary finding (that deserves further examination) that higher aerosol concentrations do not necessarily lead to convective invigoration (as evaluated by high-percentiles of vertical velocity at a single mid-tropospheric layer), despite their impact on static stability, can be explained by the fact that under equilibrium conditions, the environmental temperature profile is strongly coupled with convection. As a result, buoyancy and vertical velocities in clouds are unlikely to be influenced by the amount of latent heating from convection (Seeley & Romps, 2016).

Building on the data set and insights from this study, future research could explore the effects of aerosols on cloud feedback and climate sensitivity (Dagan, 2022a), the response of vertical velocity in clouds at various atmospheric levels and stages of development (Marinescu et al., 2021), and the influence of aerosols on different cloud regimes within the RCE framework (Lorian & Dagan, 2024). Additionally, as phase two of RCEMIP focuses on SST-forced circulations (i.e., Mock-Walker simulations; Wing et al. (2024)), future work could examine the impact of ACI on these large-scale circulations (Dagan et al., 2023). The publicly available data set presented in this study provides a valuable resource for advancing our understanding of aerosol-cloud interactions and could be highly beneficial to the scientific community.

Conflict of Interest

The authors declare no conflicts of interest relevant to this study.

Data Availability Statement

All simulation data are stored and can be accessed on the U.K. CEDA JASMIN supercomputer (https://jasmin.ac.uk). The data presented in this paper is publicly available for download from (Dagan, 2025): https://gws-access.jasmin.ac.uk/public/gewex_gap.

References

Abbott, T. H., & Cronin, T. W. (2021). Aerosol invigoration of atmospheric convection through increases in humidity. *Science*, *371*(6524), 83–85. https://doi.org/10.1126/science.abc5181

Albrecht, B. A. (1989). Aerosols, cloud microphysics, and fractional cloudiness. *Science*, *245*(4923), 1227–1230. https://doi.org/10.1126/science.245.4923.1227

Bellouin, N., Quaas, J., Gryspeerdt, E., Kinne, S., Stier, P., Watson-Parris, D., et al. (2020). Bounding global aerosol radiative forcing of climate change. *Reviews of Geophysics*, *58*(1), e2019RG000660. https://doi.org/10.1029/2019rg000660

Beydoun, H., & Hoose, C. (2019). Aerosol-cloud-precipitation interactions in the context of convective self-aggregation. *Journal of Advances in Modeling Earth Systems*, *11*(4), 1066–1087. https://doi.org/10.1029/2018ms001523

Biagioli, G., & Tompkins, A. M. (2023). Measuring convective organization. *Journal of the Atmospheric Sciences*, *80*(12), 2769–2789. https://doi.org/10.1175/jas-d-23-0103.1

Bony, S., Bellon, G., Klocke, D., Sherwood, S., Fermepin, S., & Denvil, S. (2013). Robust direct effect of carbon dioxide on tropical circulation and regional precipitation. *Nature Geoscience*, *6*(6), 447–451. https://doi.org/10.1038/ngeo1799

Bony, S., Stevens, B., Coppin, D., Becker, T., Reed, K. A., Voigt, A., & Medeiros, B. (2016). Thermodynamic control of anvil cloud amount. *Proceedings of the National Academy of Sciences of the United States of America*, *113*(32), 8927–8932. https://doi.org/10.1073/pnas.1601472113

Bony, S., Stevens, B., Frierson, D. M., Jakob, C., Kageyama, M., Pincus, R., et al. (2015). Clouds, circulation and climate sensitivity. *Nature Geoscience*, *8*(4), 261–268. https://doi.org/10.1038/ngeo2398

Choudhury, G., & Tesche, M. (2023). A first global height-resolved cloud condensation nuclei data set derived from spaceborne lidar measurements. *Earth System Science Data Discussions*, *2023*(8), 1–22. https://doi.org/10.5194/essd-15-3747-2023

Christensen, M. W., Gettelman, A., Cermak, J., Dagan, G., Diamond, M., Douglas, A., et al. (2022). Opportunistic experiments to constrain aerosol effective radiative forcing. *Atmospheric Chemistry and Physics*, *22*(1), 641–674. https://doi.org/10.5194/acp-22-641-2022

Christensen, M. W., Jones, W. K., & Stier, P. (2020). Aerosols enhance cloud lifetime and brightness along the stratus-to-cumulus transition. *Proceedings of the National Academy of Sciences of the United States of America*, *117*(30), 17591–17598. https://doi.org/10.1073/pnas.1921231117

Cotton, W. R., Pielke Sr, R., Walko, R., Liston, G., Tremback, C., Jiang, H., et al. (2003). Rams 2001: Current status and future directions. *Meteorology and Atmospheric Physics*, *82*(1–4), 5–29. https://doi.org/10.1007/s00703-001-0584-9

Dagan, G. (2022a). Equilibrium climate sensitivity increases with aerosol concentration due to changes in precipitation efficiency. *Atmospheric Chemistry and Physics*, *22*(24), 15767–15775. https://doi.org/10.5194/acp-22-15767-2022

Dagan, G. (2022b). Sub-tropical aerosols enhance tropical cloudiness–a remote aerosol-cloud lifetime effect. *Journal of Advances in Modeling Earth Systems*, *14*(12), e2022MS003368. https://doi.org/10.1029/2022ms003368

Dagan, G. (2024). Large-scale tropical circulation intensification by aerosol effects on clouds. *Geophysical Research Letters*, *51*(7), e2024GL109015. https://doi.org/10.1029/2024gl109015

Dagan, G. (2025). Data for the paper: RCEMIP-ACI: Aerosol-Cloud Interactions in a Multimodel Ensemble of Radiative-Convective Equilibrium Simulations [Dataset]. https://gws-access.jasmin.ac.uk/public/gewex_gap/

Dagan, G., & Eytan, E. (2024). The potential of absorbing aerosols to enhance extreme precipitation. *Geophysical Research Letters*, *51*(10), e2024GL108385. https://doi.org/10.1029/2024gl108385

Dagan, G., Koren, I., Altaratz, O., & Heiblum, R. H. (2017). Time-dependent, non-monotonic response of warm convective cloud fields to changes in aerosol loading. *Atmospheric Chemistry and Physics*, *17*(12), 7435–7444. https://doi.org/10.5194/acp-17-7435-2017

Dagan, G., & Stier, P. (2020). Constraint on precipitation response to climate change by combination of atmospheric energy and water budgets. *npj Climate and Atmospheric Science*, *3*(1), 1–5. https://doi.org/10.1038/s41612-020-00137-8

Dagan, G., Stier, P., Dingley, B., & Williams, A. I. (2022). Examining the regional co-variability of the atmospheric water and energy imbalances in different model configurations—Linking clouds and circulation. *Journal of Advances in Modeling Earth Systems*, *14*(6), e2021MS002951. https://doi.org/10.1029/2021ms002951

Dagan, G., Stier, P., Spill, G., Herbert, R., Heikenfeld, M., van den Heever, S. C., & Marinescu, P. J. (2022). Boundary conditions representation can determine simulated aerosol effects on convective cloud fields. *Communications Earth & Environment*, *3*(1), 1–7. https://doi.org/10.1038/s43247-022-00399-5

Dagan, G., Yeheskel, N., & Williams, A. I. (2023). Radiative forcing from aerosol–cloud interactions enhanced by large-scale circulation adjustments. *Nature Geoscience*, *16*(12), 1092–1098. https://doi.org/10.1038/s41561-023-01319-8

Diamond, M. S., Director, H. M., Eastman, R., Possner, A., & Wood, R. (2020). Substantial cloud brightening from shipping in subtropical low clouds. *AGU Advances*, *1*(1), e2019AV000111. https://doi.org/10.1029/2019av000111

Dingley, B., Dagan, G., & Stier, P. (2021). Forcing convection to aggregate using diabatic heating perturbations. *Journal of Advances in Modeling Earth Systems*, *13*(10), e2021MS002579. https://doi.org/10.1029/2021ms002579

Fan, J., Rosenfeld, D., Ding, Y., Leung, L. R., & Li, Z. (2012). Potential aerosol indirect effects on atmospheric circulation and radiative forcing through deep convection. *Geophysical Research Letters*, *39*(9), L09806. https://doi.org/10.1029/2012gl051851

Fan, J., Rosenfeld, D., Zhang, Y., Giangrande, S. E., Li, Z., Machado, L. A., et al. (2018). Substantial convection and precipitation enhancements by ultrafine aerosol particles. *Science*, *359*(6374), 411–418. https://doi.org/10.1126/science.aan8461

Forster, P. M., Smith, C., Walsh, T., Lamb, W. F., Lamboll, R., Hall, B., et al. (2024). Indicators of global climate change 2023: Annual update of key indicators of the state of the climate system and human influence. *Earth System Science Data*, *16*(6), 2625–2658. https://doi.org/10.5194/essd-16-2625-2024

Gasparini, B., Atlas, R., Voigt, A., Krämer, M., & Blossey, P. N. (2025). Tropical cirrus evolution in a km-scale model with improved ice microphysics. *EGUsphere*. (preprint). https://doi.org/10.5194/egusphere-2025-203

Glassmeier, F., Hoffmann, F., Johnson, J. S., Yamaguchi, T., Carslaw, K. S., & Feingold, G. (2021). Aerosol-cloud-climate cooling overestimated by ship-track data. *Science*, *371*(6528), 485–489. https://doi.org/10.1126/science.abd3980

Goren, T., Kazil, J., Hoffmann, F., Yamaguchi, T., & Feingold, G. (2019). Anthropogenic air pollution delays marine stratocumulus breakup to open cells. *Geophysical Research Letters*, *46*(23), 14135–14144. https://doi.org/10.1029/2019gl085412

Harris, L., Zhou, L., Lin, S.-J., Chen, J.-H., Chen, X., Gao, K., et al. (2020). GFDL SHiELD: A unified system for weather-to-seasonal prediction. *Journal of Advances in Modeling Earth Systems*, *12*(10), e2020MS002223. https://doi.org/10.1029/2020ms002223

Held, I. M., Hemler, R. S., & Ramaswamy, V. (1993). Radiative-convective equilibrium with explicit two-dimensional moist convection. *Journal of the Atmospheric Sciences*, *50*(23), 3909–3927. https://doi.org/10.1175/1520-0469(1993)050<3909:rcewet>2.0.co;2

Heus, T., van Heerwaarden, C. C., Jonker, H. J., Pier Siebesma, A., Axelsen, S., Van Den Dries, K., et al. (2010). Formulation of the Dutch atmospheric large-eddy simulation (DALES) and overview of its applications. *Geoscientific Model Development*, *3*(2), 415–444. https://doi.org/10.5194/gmd-3-415-2010

Igel, A. L., & van den Heever, S. C. (2021). Invigoration or enervation of convective clouds by aerosols? *Geophysical Research Letters*, *48*(16), e2021GL093804. https://doi.org/10.1029/2021gl093804

Jakob, C., Singh, M., & Jungandreas, L. (2019). Radiative convective equilibrium and organized convection: An observational perspective. *Journal of Geophysical Research: Atmospheres*, *124*(10), 5418–5430. https://doi.org/10.1029/2018jd030092

Khairoutdinov, M. F., & Randall, D. A. (2003). Cloud resolving modeling of the ARM summer 1997 IOP: Model formulation, results, uncertainties, and sensitivities. *Journal of the Atmospheric Sciences*, *60*(4), 607–625. https://doi.org/10.1175/1520-0469(2003)060<0607:crmota>2.0.co;2

Koren, I., Dagan, G., & Altaratz, O. (2014). From aerosol-limited to invigoration of warm convective clouds. *Science*, *344*(6188), 1143–1146. https://doi.org/10.1126/science.1252595

Lac, C., Chaboureau, J.-P., Masson, V., Pinty, J.-P., Tulet, P., Escobar, J., et al. (2018). Overview of the Meso-NH model version 5.4 and its applications. *Geoscientific Model Development*, *11*(5), 1929–1969. https://doi.org/10.5194/gmd-11-1929-2018

Latham, J., Bower, K., Choularton, T., Coe, H., Connolly, P., Cooper, G., et al. (2012). Marine cloud brightening. *Philosophical Transactions of the Royal Society A: Mathematical, Physical and Engineering Sciences*, *370*(1974), 4217–4262. https://doi.org/10.1098/rsta.2012.0086

Lebo, Z. (2018). A numerical investigation of the potential effects of aerosol-induced warming and updraft width and slope on updraft intensity in deep convective clouds. *Journal of the Atmospheric Sciences*, *75*(2), 535–554. https://doi.org/10.1175/jas-d-16-0368.1

Lorian, S., & Dagan, G. (2024). On the sensitivity of aerosol–cloud interactions to changes in sea surface temperature in radiative–convective equilibrium. *Atmospheric Chemistry and Physics*, *24*(16), 9323–9338. https://doi.org/10.5194/acp-24-9323-2024

Lutsko, N. J., & Cronin, T. W. (2018). Increase in precipitation efficiency with surface warming in radiative-convective equilibrium. *Journal of Advances in Modeling Earth Systems*, *10*(11), 2992–3010. https://doi.org/10.1029/2018ms001482

Manabe, S., & Wetherald, R. T. (1967). Thermal equilibrium of the atmosphere with a given distribution of relative humidity. *Journal of the Atmospheric Sciences*, *24*(3), 241–259. https://doi.org/10.1175/1520-0469(1967)024<0241:teotaw>2.0.co;2

Marinescu, P. J., Van Den Heever, S. C., Heikenfeld, M., Barrett, A. I., Barthlott, C., Hoose, C., et al. (2021). Impacts of varying concentrations of cloud condensation nuclei on deep convective cloud updrafts—A multimodel assessment. *Journal of the Atmospheric Sciences*, *78*(4), 1147–1172. https://doi.org/10.1175/jas-d-20-0200.1

Medeiros, B., Stevens, B., & Bony, S. (2015). Using aquaplanets to understand the robust responses of comprehensive climate models to forcing. *Climate Dynamics*, *44*(7–8), 1957–1977. https://doi.org/10.1007/s00382-014-2138-0

Morrison, H., Curry, J., & Khvorostyanov, V. (2005). A new double-moment microphysics parameterization for application in cloud and climate models. Part I: Description. *Journal of the Atmospheric Sciences*, *62*(6), 1665–1677. https://doi.org/10.1175/jas3446.1

Morrison, H., & Milbrandt, J. A. (2015). Parameterization of cloud microphysics based on the prediction of bulk ice particle properties. Part I: Scheme description and idealized tests. *Journal of the Atmospheric Sciences*, *72*(1), 287–311. https://doi.org/10.1175/jas-d-14-0065.1

Muller, C. J., & Held, I. M. (2012). Detailed investigation of the self-aggregation of convection in cloud-resolving simulations. *Journal of the Atmospheric Sciences*, *69*(8), 2551–2565. https://doi.org/10.1175/jas-d-11-0257.1

Pope, K. N., Holloway, C. E., Jones, T. R., & Stein, T. H. M. (2023). Radiation, clouds, and self-aggregation in RCEMIP simulations. *Journal of Advances in Modeling Earth Systems*, *15*(2), e2022MS003317. https://doi.org/10.1029/2022ms003317

Romps, D. M. (2008). The dry-entropy budget of a moist atmosphere. *Journal of the Atmospheric Sciences*, *65*(12), 3779–3799. https://doi.org/10.1175/2008jas2679.1

Romps, D. M., Latimer, K., Zhu, Q., Jurkat-Witschas, T., Mahnke, C., Prabhakaran, T., et al. (2023). Air pollution unable to intensify storms via warm-phase invigoration. *Geophysical Research Letters*, *50*(2), e2022GL100409. https://doi.org/10.1029/2022gl100409

Rosenfeld, D., Lohmann, U., Raga, G. B., O'Dowd, C. D., Kulmala, M., Fuzzi, S., et al. (2008). Flood or drought: How do aerosols affect precipitation? *Science*, *321*(5894), 1309–1313. https://doi.org/10.1126/science.1160606

Saleeby, S. M., & van den Heever, S. C. (2013). Developments in the CSU-RAMS aerosol model: Emissions, nucleation, regeneration, deposition, and radiation. *Journal of Applied Meteorology and Climatology*, *52*(12), 2601–2622. https://doi.org/10.1175/jamc-d-12-0312.1

Seeley, J. T., & Romps, D. M. (2016). Tropical cloud buoyancy is the same in a world with or without ice. *Geophysical Research Letters*, *43*(7), 3572–3579. https://doi.org/10.1002/2016gl068583

Sheffield, A. M., Saleeby, S. M., & van den Heever, S. C. (2015). Aerosol-induced mechanisms for cumulus congestus growth. *Journal of Geophysical Research: Atmospheres*, *120*(17), 8941–8952. https://doi.org/10.1002/2015jd023743

Silvers, L. G., Reed, K. A., & Wing, A. A. (2023). The response of the large-scale tropical circulation to warming. *Journal of Advances in Modeling Earth Systems*, *15*(3), e2021MS002966. https://doi.org/10.1029/2021ms002966

Singh, M. S., & O'Gorman, P. A. (2013). Influence of entrainment on the thermal stratification in simulations of radiative-convective equilibrium. *Geophysical Research Letters*, *40*(16), 4398–4403. https://doi.org/10.1002/grl.50796

Skamarock, W. C., Klemp, J. B., Dudhia, J., Gill, D. O., Barker, D. M., Duda, M. G., et al. (2008). A description of the advanced research WRF version 3. *NCAR technical note*, *475*(125), 10–5065.

Sobel, A. H., Nilsson, J., & Polvani, L. M. (2001). The weak temperature gradient approximation and balanced tropical moisture waves. *Journal of the Atmospheric Sciences*, *58*(23), 3650–3665. https://doi.org/10.1175/1520-0469(2001)058<3650:twtgaa>2.0.co;2

Spill, G., Stier, P., Field, P. R., & Dagan, G. (2021). Contrasting responses of idealised and realistic simulations of shallow cumuli to aerosol perturbations. *Geophysical Research Letters*, *48*(13), e2021GL094137. https://doi.org/10.1029/2021gl094137

Squires, P. (1958). The microstructure and colloidal stability of warm clouds: Part I—The relation between structure and stability. *Tellus*, *10*(2), 256–261. https://doi.org/10.3402/tellusa.v10i2.9228

Stauffer, C., & Wing, A. (2023). Explicitly resolved cloud feedbacks in the radiative-convective equilibrium model intercomparison project. *Journal of Advances in Modeling Earth Systems*, *15*(11), e2023MS003738. https://doi.org/10.1029/2023ms003738

Stauffer, C. L., & Wing, A. A. (2024). How does organized convection impact explicitly resolved cloud feedbacks in the radiative-convective equilibrium model intercomparison project? *Journal of Advances in Modeling Earth Systems*, *16*(10), e2023MS003924. https://doi.org/10.1029/2023ms003924

Stephens, G. L., Van Den Heever, S., & Pakula, L. (2008). Radiative–convective feedbacks in idealized states of radiative–convective equilibrium. *Journal of the Atmospheric Sciences*, *65*(12), 3899–3916. https://doi.org/10.1175/2008jas2524.1

Stevens, B., & Feingold, G. (2009). Untangling aerosol effects on clouds and precipitation in a buffered system. *Nature*, *461*(7264), 607–613. https://doi.org/10.1038/nature08281

Stier, P., van den Heever, S. C., Christensen, M. W., Gryspeerdt, E., Dagan, G., Saleeby, S. M., et al. (2024). Multifaceted aerosol effects on precipitation. *Nature Geoscience*, *17*(8), 719–732. https://doi.org/10.1038/s41561-024-01482-6

Tompkins, A. M., & Craig, G. C. (1998). Radiative–convective equilibrium in a three-dimensional cloud-ensemble model. *Quarterly Journal of the Royal Meteorological Society*, *124*(550), 2073–2097. https://doi.org/10.1002/qj.49712455013

Tompkins, A. M., & Semie, A. G. (2017). Organization of tropical convection in low vertical wind shears: Role of updraft entrainment. *Journal of Advances in Modeling Earth Systems*, *9*(2), 1046–1068. https://doi.org/10.1002/2016ms000802

Twomey, S. (1959). The nuclei of natural cloud formation part II: The supersaturation in natural clouds and the variation of cloud droplet concentration. *Geofisica pura e applicata*, *43*(1), 243–249. https://doi.org/10.1007/bf01993560

Twomey, S. (1974). Pollution and the planetary albedo. *Atmospheric Environment*, *8*(12), 1251–1256. https://doi.org/10.1016/0004-6981(74)90004-3

van den Heever, S. C., Stephens, G. L., & Wood, N. B. (2011). Aerosol indirect effects on tropical convection characteristics under conditions of radiative–convective equilibrium. *Journal of the Atmospheric Sciences*, *68*(4), 699–718. https://doi.org/10.1175/2010jas3603.1

Van Heerwaarden, C. C., Van Stratum, B. J., Heus, T., Gibbs, J. A., Fedorovich, E., & Mellado, J. P. (2017). Microhh 1.0: A computational fluid dynamics code for direct numerical simulation and large-eddy simulation of atmospheric boundary layer flows. *Geoscientific Model Development*, *10*(8), 3145–3165. https://doi.org/10.5194/gmd-10-3145-2017

Varble, A. (2018). Erroneous attribution of deep convective invigoration to aerosol concentration. *Journal of the Atmospheric Sciences*, *75*(4), 1351–1368. https://doi.org/10.1175/jas-d-17-0217.1

Varble, A. C., Igel, A. L., Morrison, H., Grabowski, W. W., & Lebo, Z. J. (2023). Opinion: A critical evaluation of the evidence for aerosol invigoration of deep convection. *Atmospheric Chemistry and Physics*, *23*(21), 13791–13808. https://doi.org/10.5194/acp-23-13791-2023

Wall, C. J., Norris, J. R., Possner, A., McCoy, D. T., McCoy, I. L., & Lutsko, N. J. (2022). Assessing effective radiative forcing from aerosol–cloud interactions over the global ocean. *Proceedings of the National Academy of Sciences of the United States of America*, *119*(46), e2210481119. https://doi.org/10.1073/pnas.2210481119

Weger, R., Lee, J., Zhu, T., & Welch, R. (1992). Clustering, randomness and regularity in cloud fields: 1. Theoretical considerations. *Journal of Geophysical Research*, *97*(D18), 20519–20536. https://doi.org/10.1029/92jd02038

Williams, E., Rosenfeld, D., Madden, N., Gerlach, J., Gears, N., Atkinson, L., et al. (2002). Contrasting convective regimes over the amazon: Implications for cloud electrification. *Journal of Geophysical Research*, *107*(D20), LBA–50. https://doi.org/10.1029/2001jd000380

Wing, A. A., Reed, K. A., Satoh, M., Stevens, B., Bony, S., & Ohno, T. (2018). Radiative–convective equilibrium model intercomparison project. *Geoscientific Model Development*, *11*(2), 793–813. https://doi.org/10.5194/gmd-11-793-2018

Wing, A. A., Silvers, L. G., & Reed, K. A. (2024). RCEMIP-II: Mock-walker simulations as phase ii of the radiative-convective equilibrium model intercomparison project. *Geoscientific Model Development*, *17*(16), 6195–6225. https://doi.org/10.5194/gmd-17-6195-2024

Wing, A. A., Stauffer, C. L., Becker, T., Reed, K. A., Ahn, M.-S., Arnold, N. P., et al. (2020). Clouds and convective self-aggregation in a multimodel ensemble of radiative-convective equilibrium simulations. *Journal of Advances in Modeling Earth Systems*, *12*(9), e2020MS002138. https://doi.org/10.1029/2020ms002138

Zang, L., Rosenfeld, D., Pan, Z., Mao, F., Zhu, Y., Lu, X., & Gong, W. (2023). Observing aerosol primary convective invigoration and its meteorological feedback. *Geophysical Research Letters*, *50*(12), e2023GL104151. https://doi.org/10.1029/2023gl104151

Zängl, G., Reinert, D., Rípodas, P., & Baldauf, M. (2015). The ICON (ICOsahedral non-hydrostatic) modelling framework of DWD and MPI-M: Description of the non-hydrostatic dynamical core. *Quarterly Journal of the Royal Meteorological Society*, *141*(687), 563–579. https://doi.org/10.1002/qj.2378

Zhang, Y., Fan, J., Li, Z., & Rosenfeld, D. (2021). Impacts of cloud microphysics parameterizations on simulated aerosol–cloud interactions for deep convective clouds over Houston. *Atmospheric Chemistry and Physics*, *21*(4), 2363–2381. https://doi.org/10.5194/acp-21-2363-2021